molecular microbiology

Spatial separation of FtsZ and FtsN during cell division

Journal:	*Molecular Microbiology*
Manuscript ID	MMI-2017-16695.R2
Manuscript Type:	Research Article
Date Submitted by the Author:	n/a
Complete List of Authors:	Söderström, Bill; Okinawa Institute of Science and Technology, Structural Cellular Biology Unit Chan, Helena; Okinawa Institute of Science and Technology, Structural Cellular Biology Unit Shilling, Patrick; Stockholm University, Biochemistry and Biophysics Skoglund, Ulf; Okinawa Institute of Science and Technology, Structural Cellular Biology Unit Daley, Daniel; Stockholm University, Biochemistry and Biophysics
Key Words:	cell division, super-resolution microscopy, peptidoglycan biosynthesis, FtsZ, FtsN

Spatial separation of FtsZ and FtsN during cell division

Bill Söderström[1*], Helena Chan[1], Patrick J. Shilling[2], Ulf Skoglund[1] and Daniel O. Daley[2*]

[1]Structural Cellular Biology Unit
Okinawa Institute of Science and Technology
Okinawa 904-0495
Japan

[2]Department of Biochemistry and Biophysics
Stockholm University,
Stockholm 106 91
Sweden

Address correspondence to:
Bill Söderström, bill.soederstroem@oist.jp; Tel +81 8064837515
Or
Daniel Daley, ddaley@dbb.su.se; Tel +46 8 162 910

Key words: *E. coli*, cell division, FtsZ, FtsN, super-resolution microscopy, gSTED, SIM

Summary

The division of *Escherichia coli* is mediated by a collection of some 34 different proteins that are recruited to the division septum and are thought to assemble into a macromolecular complex known as 'the divisome'. Herein we have endeavored to better understand the structure of the divisome by imaging two of its core components; FtsZ and FtsN. Super resolution microscopy (SIM and gSTED) indicated that both proteins are localized in large assemblies, which are distributed around the division septum (i.e. forming a discontinuous ring). Although the rings had similar radii prior to constriction, the individual densities were often spatially separated circumferentially. As the cell envelope constricted, the discontinuous ring formed by FtsZ moved inside the discontinuous ring formed by FtsN. The radial and circumferential separation observed in our images indicates that the majority of FtsZ and FtsN molecules are organized in different macromolecular assemblies, rather than in large super-complex. This conclusion was supported by Fluorescence Recovery After Photobleaching (FRAP) measurements, which indicated that the dynamic behavior of the two macromolecular assemblies was also fundamentally different. Taken together, the data indicates that constriction of the cell envelope is brought about by (at least) two spatially separated complexes.

Introduction

In *Escherichia coli*, at least thirty-four different proteins are recruited to the septum at the onset of division (de Boer, 2010). Ten of these proteins are thought to have major roles in constricting the mother cell and separating the daughter cells, as they are essential for cell viability (i.e. FtsZ, FtsA, ZipA, FtsK, FtsQ, FtsL, FtsB, FtsW, FtsI and FtsN) (Haeusser & Margolin, 2016, de Boer, 2010). Details of how the essential division proteins are recruited to the septum, a process often referred to as 'assembly', have been revealed through decades of research (den Blaauwen *et al.*, 2017). Thousands of molecules of FtsZ are corralled, then polymerized and bundled into filaments that are tethered to the inner membrane by FtsA and ZipA (Haeusser & Margolin, 2016, Erickson *et al.*, 2010). This intermediate structure is often referred to as the Z-ring (or proto-ring) on account of the fact that it resembles a ring when analyzed by fluorescence microscopy (Rowlett & Margolin, 2015). The Z-ring subsequently acts as an assembly platform for proteins involved in chromosome partitioning (e.g. FtsK) and peptidoglycan (PG) synthesis (e.g. FtsQ, FtsL, FtsW, FtsI, FtsN), which are recruited after a time delay (Aarsman *et al.*, 2005). Once all essential proteins have arrived at the septum, it is assumed that they assemble into a single macromolecular complex, which is referred to as the divisome (see (Trip & Scheffers, 2015) and references therein). Although the divisome has yet to be isolated, its existence is based on three main lines of evidence:

1. Experiments showing that the recruitment of proteins to the septum is often dependent on the existence of upstream proteins (Goehring & Beckwith, 2005).

2. Protein: protein interaction studies that indicate a high level of connectivity between proteins (Alexeeva *et al.*, 2010, Egan & Vollmer, 2013, Pazos *et al.*, 2013, Buddelmeijer & Beckwith, 2004, Muller *et al.*, 2007, Fraipont *et al.*, 2011, Karimova *et al.*, 2005, Di Lallo *et al.*, 2003).
3. The identification of a 1MDa complex containing some divisome proteins (Trip & Scheffers, 2015).

Constriction of the cell envelope begins once FtsN has arrived at the division septum (Weiss, 2015). It is powered by the constriction of FtsZ polymers in the cytoplasm (Osawa *et al.*, 2008, Osawa *et al.*, 2009, Osawa & Erickson, 2013), and the inward growth of the PG layer in the periplasm (Meier & Goley, 2014, den Blaauwen *et al.*, 2017, Xiao & Goley, 2016, Coltharp & Xiao, 2017). A compelling model for how the constriction of FtsZ polymers and PG synthesis are coordinated has been recently proposed (Yang *et al.*, 2017). This model postulates that FtsZ polymers swirl around the division site using a treadmilling mechanism. The treadmilling of FtsZ modulates the circumferential speed of proteins involved in PG synthesis, resulting in the in-growth of PG at sites where FtsZ polymers are actively constricting. Currently the molecular mechanism(s) by which the Z-ring modulates the PG synthesizing machinery is not understood, but it is implied that they are physically connected (Yang *et al.*, 2017, Schoenemann & Margolin, 2017).

High-resolution information on the structural architecture of the divisome would help to determine if FtsZ is in fact physically coupled to the PG synthesizing machinery. Our current view of the divisome structure is based on super-resolution imaging of fluorescently labeled FtsZ, FtsA and ZipA,

which revealed that these three proteins form patchy ring structures, with bead-like densities that often overlap (Strauss *et al.*, 2012, Rowlett & Margolin, 2014). The bead-like densities represent filaments that are each ~ 100 nm long and that together span the circumference of the septum (Coltharp *et al.*, 2016). It has been largely assumed that other divisome proteins are physically associated with these filaments throughout constriction. However, recent studies have suggested that proteins in the Z-ring are spatially separated from and proteins involved in PG synthesis machinery (Söderström *et al.*, 2016, Buss *et al.*, 2015). Our goals in this study were to confirm this separation, to determine when it happened, and better understand how it affected the ability of the Z-ring to co-ordinate the localization of the PG synthesizing machinery.

Results

The Z-ring and the PG synthesizing machinery are visibly separated at the septum

To confirm that the Z-ring and the PG synthesizing machinery were separated at the septum during constriction, we ectopically expressed FtsZ-GFP (a marker for the Z-ring) and mCherry-FtsN (a marker for the PG synthesizing machinery) in the *E. coli* strain MG1655. Live cells were then trapped in microholes made in agarose beds as previously described (Bisson-Filho *et al.*, 2017) (Fig. 1A). Initially cells were imaged by dual-color SIM, which has a resolution of ~ 100 nm (Gustafsson, 2000). This approach allowed us to obtain an unhindered view of the divisome along the longitudinal axis of the cell, without the need for 3D reconstructions from 2D images. For both FtsZ-

GFP and mCherry-FtsN we observed fluorescent rings (Fig. 1B). In cells where the radius of the FtsZ-GFP was > 450 nm we observed that the radius of the mCherry-FtsN signal appeared to be similar (Fig. 1B, left panel). We reason that these cells had only just begun to constrict, as the radius of an unconstricted cell is approximately 500 nm (Supporting Information Fig. S3). For cells where the radius of FtsZ-GFP was < 450 nm we observed that the radius of mCherry-FtsN was clearly larger (Fig. 1B, right panel). Identical observations were obtained when we imaged cells co-expressing FtsZ-mNeonGreen (-mNG) and mCherry-FtsN (Fig. 1C). Although FtsZ-mNG has a mild GTPase phenotype (Yang *et al.*, 2017), it can be incorporated at the native chromosomal locus and thus function as the only source of FtsZ in the cell (Moore *et al.*, 2017). In our experiments we could confirm that FtsZ-mNG was expressed at near native levels, and that it did not degrade (Supporting Information Fig. S4). mCherry-FtsN was mildly expressed, at levels that were less than two fold more than the wild type (Supporting Information Fig. S5).

To confirm that proteins in the Z-ring were separated from proteins in the PG synthesizing machinery we imaged other proteins by dual-color SIM. When we imaged ZipA-GFP (another marker for the Z-ring) and mCherry-FtsN we observed that the radii of the fluorescence signals appeared to be similar when the width of the cell was > 450 nm, but visibly separated when the width was < 450 nm (Fig. 1D). A difference was not observed when imaging FtsZ-mNG and FtsZ-mCherry, or ZipA-GFP and FtsZ-mCherry, (Supporting Information Fig. S6). (Supporting Information Fig. S6). Similarly, the radii of the fluorescence signals from GFP-FtsI (another marker for the PG synthesizing machinery) and mCherry-FtsN remained similar throughout the

constriction process (Fig. 1E). These data are consistent with our previous observations, which indicated that proteins in the Z-ring (i.e. FtsZ, FtsA, ZipA) are radially separated from the PG synthesizing machinery (i.e. FtsQ, FtsL, FtsI, FtsN) in constricting cells (Söderström *et al.*, 2016).

Analysis of the difference in peak-to-peak radii (Δr) of the protein pairs at different stages of constriction suggested that the Z-ring was constricting faster than the ring formed by the PG synthesizing machinery (Fig. 1F - G). For example, the Δr between FtsZ and FtsN was 14.4 ± 9.7 nm at the onset of constriction (r > 450 nm), 39.6 ± 4.5 nm in the middle of constriction (r ~ 450 nm to ~ 200 nm) and 45.8 ± 5.2 nm at a later stage of constriction (r < 200 nm) (Fig. 1H). When r < 100 nm, FtsZ disassembled whilst FtsN stayed until the daughter cells separated (see (Söderström *et al.*, 2014)). Taken together, these measurements indicate that the majority of molecules in the Z-ring separate from the majority of molecules in the PG synthesizing machinery. The separation occurs at the onset of constriction and becomes increasingly larger as the envelope is constricted.

To visualize the separation in finer detail we used time-gated STimulated Emission Depletion (gSTED) nanoscopy, which has a resolution capability of ~ 35 - 40 nm (Vicidomini *et al.*, 2011, Vicidomini *et al.*, 2013). In our experimental conditions and microscopy parameters the resolution was estimated to be ~ 50 nm (Supporting Information Fig. S7). In this series of experiments, we co-expressed FtsZ-mNG from the chromosome and mStrawberry-FtsN from a plasmid and imaged their relative positions at the division site in cells trapped in microholes. Thus FtsZ-mNG was the only

source of FtsZ, whilst both the native FtsN and mStrawberry-FtsN were present. In the conditions used for the experiment, the expression of mStrawberry-FtsN was less than two fold more than the wild type (Supporting Information Fig. S5). Moreover the fusion could complement an FtsN depleted strain (Supporting Information Fig. S12). Initially gSTED imaging was done using both live and fixed cells. The dual-color gSTED images were similar using both methods; they showed that FtsZ-mNG and mStrawberry-FtsN appeared as spots that were localized around the divisome. However, to avoid motion induced blurring and relative protein motion during image acquisition, we opted to use fixed cells (Fig. 2A). Line scans along the circumference of the division site revealed that the spots were separated by stretches that were completely devoid of fluorescence (Fig. 2A). Discontinuous rings have been noted previously (Strauss *et al.*, 2012, Holden *et al.*, 2014, Coltharp *et al.*, 2016, Rowlett & Margolin, 2014).

Curiously, even though FtsZ-mNG and mStrawberry-FtsN formed discontinuous rings with similar radii, the proteins did not always co-localize (Fig. 2B). Imaging fluorescent mircobeads ruled out channel misalignment (Supporting Information Fig. S8). We therefore conclude that the vast majority of FtsZ-mNG and mStrawberry-FtsN molecules are spatially separated, even at a very early stage of constriction. gSTED imaging of mStrawberry was technically challenging, particularly in constricting cells ($r < 450$ nm). Nevertheless, were we able to confirm that FtsZ-mNG and mStrawberry-FtsN constricted into discontinuous rings with different radii (Fig. 2C - G). The Δr was on average 48.2 ± 6.5 nm ($n = 8$), which is consistent with data obtained using SIM.

Intriguingly, in some gSTED images we observed cells where the radii formed by FtsZ-mNG and mStrawberry-FtsN appeared to overlap in some sections, but not in other sections (Supporting Information Fig. S8). This observation suggests that constriction by the Z-ring is asymmetric. Similar observations have been made in other bacteria, although not *E. coli* (Yao *et al.*, 2017). Taken together the dual color gSTED images enabled us to better resolve localization of FtsZ and FtsN, and determine that the majority of molecules are spatially separated.

Hidden details of the divisome ultra-structure

The gSTED images of FtsZ-mNG indicated that the densities were often irregular. For example, while most densities were positioned along the circumference of the division site (Fig. 2C, line 1), some appeared to be oriented perpendicular to the circumference (Fig. 2C, line 2). To better understand these fine details, we analyzed single color gSTED images of cells expressing only FtsZ-mNG (Fig. 3A). Quantitative measurements revealed an average width (along the long axis of the cell) of 109 ± 14 nm (n = 10), and an average radial thickness of 80 ± 2 nm (n = 50) (Supporting Information Fig. S9). The average length of the FtsZ-mNG patches was 109 ± 4 nm (n = 158) (Fig. 3B, 3N), and the average ring coverage was 65 ± 12 %, n = 48 (Fig. 3O). Curiously, about 3 % of these patches were arranged in helical-like structures within the rings (Fig. 3C). To validate these observations, we immuno-decorated the native FtsZ in wild type cells (Fig. 3D). The average width of the ring in wild type cells was 116 ± 19 nm (n = 11) (Supporting Information Fig. S11), the radial thickness 79 ± 2 nm (n = 58), the

220 average length was 115 ± 6 (n = 102) (Fig. 3E - F, 3N) and the average ring
221 density was 53 ± 8 % (n = 48). These observations of the antibody labeled
222 FtsZ are consistent with values obtained from FtsZ-mNG. They are also
223 consistent with PALM images using FtsZ-FP fusions (Fu *et al.*, 2010, Coltharp
224 *et al.*, 2016) and *in vitro* reconstitution experiments (Huecas *et al.*, 2008,
225 Romberg *et al.*, 2001, Chen *et al.*, 2005). In wild type cells, we observed that
226 roughly 5 % of the native FtsZ patches oriented perpendicular (or nearly so) to
227 the tangent of the ring (Fig. 3F, line 1). This latter observation is consistent
228 with, although less pronounced than, anisotropy measurements on FtsZ
229 filaments (Si *et al.*, 2013). It could be caused by internal disorganization in the
230 Z-ring, or by the fact that the Z-ring follows local membrane deformations.
231
232 We also characterized the septal organization of FtsN at a nanometer scale,
233 as this had not been done previously. For these experiments, we analyzed
234 images of mCitrine-FtsN and antibody labeled FtsN, again using gSTED.
235 mCitrine is a yellow fluorescent protein that has superior STED properties
236 (Vicidomini *et al.*, 2011, Hein *et al.*, 2008), and it was therefore used instead
237 of mStrawberry. In the conditions used for the experiment, the expression of
238 mCitrine-FtsN was less than two fold more than the wild type (Supporting
239 Information Fig. S5). Moreover the fusion could complement an FtsN depleted
240 strain (Supporting Information Fig. S12). The average width of mCitrine-FtsN
241 at the septum (along the long axis) was 127 ± 8 nm (n = 8) (Supporting
242 Information Fig. S9), the radial filament thickness of the densities in the ring
243 was 101 ± 2 nm (n = 46) (Supporting Information Fig. S9), and the length of
244 the filaments was 106 ± 3 nm (n = 190) (Fig. 3G - H). The average ring

coverage was 79 ± 7 % (n = 51) (Fig. 3O). Densities of antibody labeled FtsN were similar to those observed from mCitrine-FtsN, ruling out artifacts caused by mild overexpression or the use of tags. The average width of antibody labeled FtsN was 126 ± 9 nm (n = 9) (Supporting Information Fig. S13), the radial filament thickness 102 ± 2 nm (n = 39) and length 117 ± 3 nm (n = 182) (Fig. 3K - M). The ring coverage was 81 ± 4 % (n = 26) (Fig. 3O). Although the dimensions of FtsN densities were comparable to those formed by FtsZ, they occupied approximately 20 % more area at the division site.

Taken together the single color gSTED images allowed us to quantify the dimensions of individual densities of FtsZ and FtsN on a nanometer scale. The subsequent analyses revealed that both FtsZ and FtsN are in large protein assemblies (larger than the resolution achievable in our gSTED). Since our previous data had established that these densities are spatially separated, we reason that there are at least two types of large assemblies (or polymers) present at the septum; one containing FtsZ and the other containing FtsN

Movement of the Z-ring and the proteins involved in PG synthesis around the division site is not affected by separation

Our observation that FtsZ and FtsN are radially separated during constriction raises an interesting question; does the PG synthesizing machinery continue to move around the septum even after separation from the Z-ring? To monitor the movement of proteins we performed time-lapse SIM imaging on cells simultaneously expressing a chromosomal FtsZ-GFP fusion and mCherry-FtsN expressed from a plasmid. We observed that the fluorescence densities

did indeed move around the circumference of the division site (Fig. 4A; Supporting Movie S1), and that these movements were maintained even when the radius of FtsZ-GFP was clearly smaller than that of mCherry-FtsN (Fig. 4B; Supporting Movie S2). Analogous observations were made in cells co-expressing ZipA-GFP and mCherry-FtsN, confirming that the separation does not limit FtsN movement (Supporting Movies S3 and S4). Although, the time resolution in our SIM system was not adequate to accurately determine the velocity of the moving clusters, kymographs obtained from epi-fluorescence time-lapse images using a higher time resolution (2 sec / image) gave an estimated velocity for FtsZ and ZipA of 29 ± 5 nm/sec (n = 23) and 23 ± 11 nm/sec (n = 9), respectively (Supporting Information Fig. S14). Due to the fact that the mCherry-FtsN assemblies were more confluent within the rings, we were unable to extract a reliable estimation of their velocity (Supporting Information Fig. S14). Nevertheless, our observations indicate that both FtsZ and FtsN move around the circumference of the septum, even when the radii of the respective rings are separated by as much as 50 nm. This observation is consistent with recent literature, which noted that the Z-ring (specifically FtsZ and FtsA) and proteins involved in PG synthesis (specifically FtsI) traverse the circumference of the septum (Yang *et al.*, 2017, Bisson-Filho *et al.*, 2017). We must stress though, that our data do not provide any indication as to whether FtsZ treadmilling is physically driving the circular motion of proteins involved in PG synthesis. Although this scenario seems unlikely, given the spatial separation we have observed, it is formally possible. For example, if another protein or proteins was physically linking

FtsZ to the proteins involved in PG synthesis. Or if there were small populations of FtsZ and FtsN, that eluded detection in our experiments.

Movement of the FtsZ and FtsN is mechanistically different

To better understand the underlying mechanism(s) by which FtsZ and FtsN exchange protein subunits at the division site, we monitored their respective dynamics using confocal Fluorescence Recovery After Photobleaching (FRAP). In these experiments, we trapped live cells co-expressing FtsZ-GFP and mCherry-FtsN in microholes, then photobleached sections of their respective rings and monitored the recovery of the signal. Fig. 5A shows an example where a quarter of a ring was bleached and the subsequent recovery monitored over time. This experiment allowed us to determine how fast fluorescent molecules re-enter the bleached areas of the rings, which gives an indication of their exchange rate. When quarter rings were bleached, we observed that the average $t_{1/2}$ of FtsZ-GFP was 3.92 ± 0.21 s and that of mCherry-FtsN was 0.80 ± 0.34 s (n = 9) (Fig. 5B).

When half rings were bleached, we observed that the $t_{1/2}$ increased proportionally, as expected for a larger area. For example, FtsZ-mNG (8.45 ± 2.21 s, n = 8), FtsZ-GFP (9.87 ± 2.52 s, n = 7), mCherry-FtsN (1.43 ± 0.52 s, n = 6) or mCitrine-FtsN (1.87 ± 0.66 s, n = 9) (Fig. 5C and Supporting Information Fig. S15). As expected, the fluorescence recovery was dependent on the diffusion of proteins in the cell, as we did not observe it when cells were fixed (Supporting Information Fig. S15). These FRAP data on FtsZ are in good agreement with published data, obtained from cells lying flat on agarose pads (9 ± 3 s, (Anderson *et al.*, 2004)). The ~ 4-5-fold faster recovery times

observed for FtsN compared to FtsZ indicate that the rate at which FtsN subunits are exchanged at the septum is faster than the rate at which FtsZ treadmills. The difference in recovery rate was not an artifact of the fluorophores, as we had used two different fluorophores for both FtsZ and FtsN.

In a separate series of FRAP experiments, we bleached all molecules except those in the top and bottom of the rings and monitored the re-appearance of fluorescence molecules (Fig. 5D - E). We observed that FtsZ-GFP fluorescence reappeared at different places throughout the bleached regions of the ring (Fig. 5D, white arrows; Supporting Movie S5). The same behavior was observed when monitoring the fluorescence recovery in cells expressing FtsZ-mNG (Fig. 5E). These data are consistent with polymer rebuilding *in vivo*, and they validate previous TIRF data that show FtsZ treadmilling *in vitro* and *in vivo* (Yang et al., 2017, Loose & Mitchison, 2014, Bisson-Filho et al., 2017).

Photobleaching large sections of the rings formed by FtsN was not feasible, since there are generally fewer proteins present in the cell. We therefore bleached half of the ring and followed the redistribution of fluorescence at a higher time resolution. Curiously, recovery of FtsN was always evenly distributed over the bleached area (Fig. 5F). Although we still do not fully understand what underlying mechanism drives subunit exchange in the PG synthesizing machinery, our data does suggest that it is different to FtsZ. FtsN subunits exchange continuously, not constrained by polarity, while on the other hand FtsZ monomers are added directionally and recovery behavior is therefore consistent with treadmilling motion.

Discussion

The division of an *E. coli* cell requires the coordinated action of at least thirty-four different proteins (Haeusser & Margolin, 2016, de Boer, 2010). It has been largely assumed that these proteins assemble into a single macromolecular complex. However, recent data from our labs suggested that, during constriction of the cell envelope, proteins in the Z-ring (FtsZ, FtsA, ZipA) were largely separated from proteins required for PG synthesis (FtsQ, FtsL, FtsI, FtsN) (Söderström & Daley, 2017, Söderström *et al.*, 2016). The separation of these different proteins into functional modules has important implications for understanding how the divisome proteins coordinate constriction of the cell envelope, so we were motivated to better understand the separation. Herein, our experiments focused on FtsZ and FtsN as they represent the Z-ring and the PG synthesizing machinery respectively. The approach we took was to co-express FtsZ and FtsN as FP fusions, then immobilize cells in a 'standing' position and image them using either dual-color SIM (live cells) or gSTED (fixed cells). gSTED images indicated that both proteins appeared as discrete densities that were organized as discontinuous rings around the septum. The dimensions of the densities were consistent with either large protein assemblies or filaments and bundles. A back of the envelope calculation based on the dimensions of the densities and the average ring coverage, indicates that there are between 13 and 18 visible FtsZ densities in an unconstricted cell. For FtsN we calculated 21 - 22 densities per unconstricted cell. Thus, there are fewer FtsZ densities in the

cell. The discontinuous rings we observed when imaging FtsZ are consistent with a number of previous studies that have used fluorescence microscopy (Rowlett & Margolin, 2014, Holden *et al.*, 2014, Strauss *et al.*, 2012, Fu *et al.*, 2010, Coltharp *et al.*, 2016, Jacq *et al.*, 2015). However, it should be noted that cryo-ET imaging has shown that FtsZ protofilaments can form both continuous ribbons around the division septum as well as largely discontinuous Z-rings (Szwedziak *et al.*, 2014, Yao *et al.*, 2017).

Significantly, our images indicated that the bulk of the FtsZ and FtsN fluorescence emission was spatially separated during constriction. At an early stage of constriction (r > 450 nm), we observed that the assemblies containing FtsZ and FtsN were distributed around the division site with a similar radius, but they did not always overlap. Once the cells started to visibly constrict (r < 450 nm), the radius of the ring formed by the FtsZ containing complexes was approximately 50 nm smaller than that of the ring formed by the FtsN containing complexes. Quantitative analysis of the SIM images indicated that the difference between the radii gradually increased as constriction progressed. The radial separation cannot be explained by topological differences between the FP moieties that were fused to FtsZ and FtsN, as these moieties were both localized to the cytoplasm and should be close to the inner membrane. Moreover, it cannot be explained by extension of the unstructured linker that separates FtsZ from its C-terminal anchor, as this linker is only 17 nm long in its fully extended conformation (Erickson *et al.*, 2010, Ohashi *et al.*, 2007). We believe that the most likely interpretation of these data is that the majority of FtsZ molecules are physically separated from the majority of the FtsN molecules. Considering that electron microscopy

images of dividing cells have indicated that the septal invagination is steep (see (Burdett & Murray, 1974a, Burdett & Murray, 1974b)), we reason that the majority of FtsZ molecules are localized at the leading edge of the invagination, whereas the majority of FtsN molecules are localized approximately 50 nm further back from the leading edge (Fig. 6).

We also explored the mechanism(s) of FtsZ and FtsN movement around the septum using a photobleaching assay. We observed that following bleaching, FtsZ recovered 4-5 times slower than FtsN. We also observed that FtsZ recovered as continuously and directionally growing polymers that were consistent with filament treadmilling behavior, whilst FtsN recovered in a fundamentally different manner. Taken together the data suggest that both FtsZ and FtsN clusters do traverse the septum, but that the majority of molecules do so within radially separated densities using different mechanisms.

The spatial separation of FtsZ and FtsN raises a simple but as of yet unresolved question; what is the divisome? For some time, the divisome has been considered as a large protein complex containing all divisome proteins. This may very well be true at an early time point in the assembly process, which we were not able to capture in our images; we assume that constriction was initiated in our experiments since FtsN was localized to the septum (Weiss, 2015). It may also be true if there is a small population of FtsZ or FtsN that has evaded detection. Or alternatively, if FtsZ and FtsN are connected by other divisome proteins. For example, FtsA is known to physically interact with both FtsZ and FtsN, and in theory, it could act as a bridge between the two.

However, we believe our data point to the existence of spatially separated protein complexes.

The existence of spatially separated assemblies that contain either FtsZ or FtsN at the septum is broadly consistent with what is known about the arrival of proteins at the division site. Specifically, that those proteins in the Z-ring arrive at the septum first, forming a scaffold that recruits proteins required for PG synthesis (Aarsman *et al.*, 2005). That FtsZ and FtsN are organized in different complexes is also consistent with studies timing the departure of proteins from the septum, which have shown that FtsZ and other proteins in the Z-ring move away from the septum prior to proteins required for PG synthesis (Söderström *et al.*, 2016, Söderström *et al.*, 2014). If the Z-ring and the proteins involved in PG synthesis were part of a single macromolecular complex, one could expect that disassembly of the scaffold would also release the proteins involved in PG synthesis. But this is not the case.

The radial separation, combined with differences in ring densities of FtsZ and FtsN has important implications for understanding how envelope constriction is coordinated. It has been recently demonstrated that treadmilling of FtsZ modulates the directional movements of FtsI (although FtsZ and FtsI did not appear to have the same average circumferential velocity), and from this data it was hypothesized that PG in-growth is stimulated at sites where FtsZ polymers are constricting (Yang *et al.*, 2017, Bisson-Filho *et al.*, 2017). However, it remains to be determined how FtsZ polymers can ‘control’ the localization of the proteins involved in PG synthesis (see (Schoenemann & Margolin, 2017, Du & Lutkenhaus, 2017, Coltharp & Xiao, 2017)). A physical coupling has been implied (Schoenemann & Margolin, 2017), and this maybe

the case, if there are small populations of molecules that have either evaded detection in our studies. Or, if molecules on the fringes of the fluorescent signals are physically interacting. However, given the spatial separation during constriction, combined with differences in ring coverage and the temporal differences in departure from the septum, this scenario is difficult to envision.

Experimental Procedures

Plasmids

Generation of fluorescent fusion proteins was performed using the Gibson assembly protocol (Gibson *et al.*, 2009) with Q5-polymerase (NEB) used as a replacement to Phusion-polymerase. Plasmids created for this study (pPS001, pHC002 and pHC004) contain a pRha67 backbone, which has a high-copy pUC origin of replication (Giacalone *et al.*, 2006). In the version of pRha67 that we used, the original ampicillin resistance marker was replaced with a kanamycin resistance marker (Hjelm *et al.*, 2015). All plasmids are listed in Supporting Information Table S1. The coding sequence for FtsZ was sourced from the K12-derived strain MC1061, while codon optimized mTagBFP, mStrawberry, and mCitrine were sourced from Genscript, Clontech and the mCitrine-N1 plasmid respectively. PCR of each fluorescent target and the respective rhamnose-inducible pRha67 plasmid (Giacalone *et al.*, 2006, Söderström *et al.*, 2016) was performed using primers listed in Supporting Information Table S2. The FtsZ-mTagBFP contains a linker sequence encoding NNNLQ, between FtsZ and mTagBFP. The mStrawberry-FtsN and

mCitrine-FtsN contain a linker sequence encoding ASEL, between the fluorescent protein and the respective divisome protein. All plasmid sequences were verified by DNA sequencing (Eurofins MWG or Fasmac, Japan).

Bacterial growth

Pre-cultures of were grown overnight in 20 ml of LB with appropriate antibiotics (Kanamycin 50 µg ml^{-1}, Ampicillin 50 µg ml^{-1}, Chloramphenicol 15 µg ml^{-1}, Spectinomycin 30 µg ml^{-1}) at 37 °C. The following morning the cultures were back-diluted 1:50 in LB, and incubated at 30 °C or 37 °C to OD_{600} 0.2-0.5. Strains expressing FtsZ-mNG were grown in M9 minimal media supplemented with 1µg ml^{-1} thiamine, 0.2 % (w/v) glucose and 0.1 % (w/v) casamino acids appropriate antibiotics when needed (Kanamycin 50 µg ml^{-1}, Ampicillin 50 µg ml^{-1}, Chloramphenicol 15 µg ml^{-1}, Spectinomycin 30 µg ml^{-1}), and incubated at 30 °C OD_{600} 0.2-0.5. For a complete list of strains and plasmids used in the work see Supporting Information Table S1.

Fluorescent protein production

Chromosomally encoded FtsZ-mNeonGreen was integrated at the native *ftsZ* locus and needed no inducer (Moore *et al.*, 2017). Chromosomally encoded FtsZ-GFP, ZipA-GFP and GFP-FtsI were induced by 2.5, 50, 5 µM IPTG, respectively (Söderström *et al.*, 2016, Söderström *et al.*, 2014). Plasmid encoded FtsZ-mTagBFP was induced by 5 mM rhamnose. Plasmid encoded mCherry-FtsN, mStrawberry-FtsN and Citrine-FtsN were induced by either 2.5 or 5 mM rhamnose. FtsZ-mCherry was induced with 0.2 % arabinose, as

493 described previously (Galli & Gerdes, 2010). Expression levels of fusion
494 proteins relative to the native protein, was assessed by Western blotting
495 (Supporting Information Fig. S4 and S11).
496
497 *Nanofabrication of the micropillar mold*
498 The approach for the micron-sized pillars was adapted from (Bisson-Filho et
499 al., 2017). Micron-scale pillars were fabricated on a Silicon (Si) substrate by
500 reactive ion etching, using a multi-step process similar to the one described in
501 (Antonov *et al.*, 2015). Briefly, a pattern of hard-baked photoresist was
502 created on a Si surface using UV lithography, to work as a mask for etching.
503 The etching was performed using an Oxford Plasmalab100 ICP180 CVD/Etch
504 system, with a mixture of SF_6 and O_2 plasma as an etchant. Increasing
505 concentration of O_2 in the mixture has two effects: (i) it improves etching
506 anisotropy, which is essential for pillar formation; (ii) it reduces Si to
507 photoresist selectivity ratio, which limits the possible height of pillars. For our
508 process the ratio of SF_6:O_2 = 1:1 was optimal. After the etching, the remaining
509 photoresist was removed by O_2 plasma treatment. Pillar arrays (1 x 1 cm or 2
510 x 2 cm) were made with one micron sized pillar every 5 micrometers, with
511 dimensions between 1.1 and 1.4 microns wide and 4.5 - 6 microns high.
512
513 *Production of microholes in agarose beds*
514 Agarose (2.5-5% w/v) was dispersed on glass slides and the silica mold was
515 placed on top. Once the agarose had solidified the mold was removed and ~
516 10 µl of live cell culture (at OD_{600} 0.2-0.5 concentrated 10x by centrifugation)
517 was applied, incubated for ~ 1 minute whereby the excess liquid was removed

518 and the agarose pad covered with a pre-cleaned cover glass (♯1.5). In order
519 to minimize the risk of motion blurring during image acquisition, each cell was
520 initially monitored using bright field and Epi/confocal fluorescence illumination
521 to verify that no visible movements were observed.
522
523 *Cell fixation, immunofluorescence and WGA labeling*
524 Cells were fixed and immunodecorated as described previously (Ogino *et al.*,
525 2004, Söderström *et al.*, 2016), with minor adjustments as follows. Briefly, 900
526 µl of ice-cold methanol was added to 100 µl of cell culture (OD_{600} ~0.2 – 0.5)
527 and incubated for 5 minutes on ice. Cells were harvested by centrifugation
528 and resuspended in 100 µl of 90 % (v/v) ice-cold methanol. For
529 immunodecoration of cells, roughly 20 µl of cell suspension applied on a cover
530 glass coated with Poly-L-Lysine or on agarose microhole beds and left for ~ 2
531 minutes before excess culture was removed. After drying, the cells were
532 treated with lysozyme solution (0.2 mg/mL lysozyme, 25 mM Tris-HCl pH 8.0,
533 50 mM glucose, 10 mM EDTA) for 5 min and then rinsed with PBSTS
534 [140 mM NaCl, 2 mM KCl, 8 mM Na_2HPO_4, 0.05% (v/v) Tween 20, 20% (w/v)
535 sucrose], before they were treated with methanol for 1 min and acetone for
536 1 min and dried. Fixed cells were incubated with 2% (w/v) bovine serum
537 albumin in PBSTS for at least 15 min. Thereafter the cells were washed with
538 PBSTS and incubated with primary antibodies against FtsZ (Rabbit, Agrisera,
539 Sweden) or FtsN (Rabbit, (Wissel & Weiss, 2004)) diluted 1:200 in the same
540 buffer for at least 1 hour at RT, or overnight at 4 °C. Oregon Green 488-
541 conjugated anti-rabbit serum (Molecular Probes) at a 1:500 dilution (in PBSTS
542 containing 2 % (w/v) BSA) was used as secondary antibody against FtsZ due

to its STED compatibility. Between each incubation, and after the last, the cells were washed at least 10 times in PBSTS. Cells on cover glasses were placed on glass slides with ~ 20 µl Moviol as mounting media and left overnight to harden before imaging, while cells in agarose microhole beds were covered with a pre-cleaned cover glass (♯1.5) and imaged directly.

For cell width determination of unconstricted cells, WGA (Wheat Germ Agglutinin) conjugated with Oregon Green 488 (f.c. 100 µm ml^{-1}) was applied to exponentially growing cells, cultures were allowed to grow for ~ 3 hours, and then fixed in either 2 % PFA (15 minutes in RT) or 90 % ice-cold methanol (5 minutes on ice). After fixation the cultures were washed 2 times in PBS and directly applied to an agarose pad before imaging.

Imaging on flat agarose beds or in microholes

Gated STED (gSTED) images were acquired on a Leica TCS SP8 STED 3X system, using a HC PL Apo 100x oil immersion objective with NA 1.40. Fluorophores were excited using a white excitation laser operated at 488 nm (for mNeonGreen and OG488) or 506 nm (for mCitrine), a STED laser line operated at 592 nm, and detection time-delay of 0.9 - 2.5 ns. mStrawberry was excited using a 574 nm laser light and depleted using a 660 nm STED laser line, and the delay-time was 0.5-0.8 ns. The total depletion laser intensity was on the order of 20-100 MW/cm^2 for all experiments. The final pixel size was 13 nm and scanning speed 600 Hz. The pinhole size was varied between 0.4-0.9 AU; a smaller pin-hole when imaging cells standing trapped in microholes and larger when imaging cells laying flat on agarose pads.

Epi-fluorescence, confocal and SIM images were acquired on either a Zeiss LSM780 or Zeiss ELYRA PS1 (both equipped with a 100X 1.46NA plan Apo oil immersion objective) with acquisition times between 0.3 and 2 sec. Time-lapse movies were recorded with intervals of 1 - 10 seconds. SIM images were acquired using ELYRA PS1 (pco.edge sCMOS camera). Pixel size 50 nm in SIM images. SIM time-lapse movies (containing either 7 or 10 frames) were recorded with time intervals between 0 sec and 5 minutes. Individual images were acquired with acquisition times between 300 and 500 ms per image (a total of 15 images were acquired per SIM image reconstruction) and subsequently reconstructed from the raw data in the ZEN2012 software. It is important to note that images in different channels in the SIM time-lapse images were acquired sequentially (total acquisition time for one channel was between ~ 7 - 10 seconds), thus the relative density (protein) localization within the rings cannot be analyzed in this way, only the relative radial overlap/separation between respectively channel can be assessed. All imaging was performed at room temperature (~23-24 °C).

Image analysis

STED images were deconvolved using Huygens Professional deconvolution software (SVI, the Netherlands). Epi-fluorescence and SIM image stacks were drift-corrected using the ImageJ plugin StackReg. Images were background subtracted using a rolling ball radius of 50. To determine the difference in radii between the Z-ring proteins and FtsN in Fig. 1, we assumed the cells to have a circular shape and line scans were drawn from 3 o'clock to 9 o'clock over the rings. The resulting peak-to-peak distance was analyzed in Origin9 Pro.

The two fluorescence maxima were fitted to Gaussians using the multiple peak analyzer function in Origin9 Pro, and from the fitted maxima the diameter was subsequently extracted. The respective ring radii were then calculated and the smaller (e.g. FtsZ) was subtracted from the larger (i.e. FtsN) in order to determine the difference in radii, Δr.

For cells imaged by gSTED the radii were estimated from a circle drawn along the maxima of the fluorescence profiles. Cluster length and width values were obtained from the entire population of cells using line scans (line size 3) over randomly selected individual protein clusters (2-4 clusters per cell) from deconvolved images. A Gaussian distribution was fitted to the intensity profiles in order to extract the Full Width at Half Maximum (FWHM). The resolution in our gSTED images was ~ 50 nm (Supporting Information Fig. S7). Clusters did not always follow the circumference of the cells therefore we always regarded the long axis as “length” and the short axis as “width”. Kymographs were generated using the ImageJ plugin KymoResliceWide applied on lines drawn long the circumference of the cells (fluorescence profile). The mean velocity was subsequently extracted manually by following individual filaments bundles over time and then converting the traveled distance from degrees to nm, as described (Loose & Mitchison, 2014). The ring coverage was estimated from line scans with lines thicker than the fluorescence signal in the radial direction. The portion of the circumference, normalized to length, which had none-zero intensity, was integrated to obtain the ring coverage in % of total ring length. Note that ~ 10 % of the normalized signal was subtracted as background, thus the presented absolute values of ring coverage may be slightly underestimated.

FRAP analysis

Confocal FRAP measurements were performed on a Zeiss LSM780 system, using a 100x 1.4NA plan Apo oil immersion objective and pinhole size of varying between 60 and 20 µm. Bleaching was performed using 100% laser power applied over the region of interest between 0.4 and 1 second, and data was collected in time intervals between 0.6 and 10 seconds. After background correction, the fluorescence intensity of the bleached region (half a ring, quarter of a ring or other) was normalized to the average ring fluorescence of an area of same size as the bleached; $F_{NORM}(t) = F_{BLEACHED}(t)/(F_{BLEACHED}(t)+ F_{UNBLEACHED}(t))$. All data was exported to Origin9 Pro and data points were fitted to the single exponential function $F(t) = F_{end} – (F_{end} – F_{start})* e^{-kt}$, where F(t) is the fluorescence intensity at time t, F_{end} is the fluorescence intensity at maximum recovery, F_{start} is the fluorescence recovery momentarily after bleaching (at t = 0), and k is a free parameter. The recovery half time was then extracted from $t_{1/2} = \ln 2 / k$. Importantly, all cells were scanned from top to bottom in order to find the division plane (in which the rings reside).

Cell length and width measurements

Cells from 1 ml cultures were harvested by centrifugation. The cultures were washed twice in 200 µl PBS before an aliquot (~ 6 µl) was placed on an agarose bed and directly imaged under bright-field illumination. Cell lengths of at least 100 cells from each strain were determined using the ROI manager in ImageJ and statistics were calculated and graphs were produced using OriginPro9.

Cryo-electron microscopy

WT cells were grown as described above. A 2 µl aliquot of cell culture was applied on glow discharged EM grids (Quantifoil, 3,5/1, Cu 200 mesh) and directly flash frozen in liquid Ethane using a FEI Vitrobot. Subsequent imaging was performed on an FEI Titan KRIOS 300 kVe electron microscope, using a nominal magnification of 22500X. Image acquisition time was 1 second, the underfocus was kept at – 8 µm. Images were resolution and contrast enhanced using the COMET (Skoglund *et al.*, 1996) software operated in 2D mode.

Western blotting

Cell extracts from a volume corresponding to 0.1 DO_{600} units were collected for different strains. The extracts were suspended in loading buffer and resolved by sodium dodecyl sulphatepolyacrylamide gel electrophoresis. Proteins were transferred to nitrocellulose membranes using a semi-dry Transfer-Blot apparatus (Bio-Rad). The membranes were blocked in 5 % (w/v) milk and probed with antisera to either FtsZ (Agrisera, Sweden), FtsN (Wissel & Weiss, 2004) or GFP (Abcam, UK).

Acknowledgements

We are grateful to Prof. Harold Erickson, Prof. Piet de Boer and Lynda Lee for sharing strains, and Prof. David Weiss for FtsN antisera. We would like to extend our gratitude to the Nanofabrication section at OIST for help with producing the micro-pillar arrays. BS is supported by JSPS KAKENHI Grant Number JP17K15694. Work in the Structural Cellular Biology Unit is funded by core subsidy funding from Okinawa Institute of Science and Technology Graduate University. DOD is supported by the Swedish Research Council and Carl Trygger stiftelse.

Conflict of interest

The Authors declare no conflicts of interest.

Author contributions

B.S and D.O.D. designed the study and conceived the experiments. H.C and P.S. contributed new reagents. B.S. performed the experiments. All authors analysed the data. B.S and D.O.D. wrote the manuscript with input from the other authors. All authors have read and approved the final version.

References

Aarsman, M.E., A. Piette, C. Fraipont, T.M. Vinkenvleugel, M. Nguyen-Disteche & T. den Blaauwen, (2005) Maturation of the *Escherichia coli* divisome occurs in two steps. *Molecular microbiology* **55**: 1631-1645.

Alexeeva, S., T.W. Gadella, Jr., J. Verheul, G.S. Verhoeven & T. den Blaauwen, (2010) Direct interactions of early and late assembling division proteins in *Escherichia coli* cells resolved by FRET. *Molecular microbiology* **77**: 384-398.

Anderson, D.E., F.J. Gueiros-Filho & H.P. Erickson, (2004) Assembly dynamics of FtsZ rings in *Bacillus subtilis* and *Escherichia coli* and effects of FtsZ-regulating proteins. *Journal of bacteriology* **186**: 5775-5781.

Antonov, P.V., M.R. Zuiddam & J.W.M. Frenken, (2015) Fabrication of high-aspect ratio silicon nanopillars for tribological experiments. *J Micro-Nanolith Mem* **14**.

Bisson-Filho, A.W., Y.P. Hsu, G.R. Squyres, E. Kuru, F. Wu, C. Jukes, Y. Sun, C. Dekker, S. Holden, M.S. VanNieuwenhze, Y.V. Brun & E.C. Garner, (2017) Treadmilling by FtsZ filaments drives peptidoglycan synthesis and bacterial cell division. *Science* **355**: 739-743.

Buddelmeijer, N. & J. Beckwith, (2004) A complex of the *Escherichia coli* cell division proteins FtsL, FtsB and FtsQ forms independently of its localization to the septal region. *Molecular microbiology* **52**: 1315-1327.

Burdett, I.D. & R.G. Murray, (1974a) Electron microscope study of septum formation in *Escherichia coli* strains B and B-r during synchronous growth. *Journal of bacteriology* **119**: 1039-1056.

Burdett, I.D. & R.G. Murray, (1974b) Septum formation in *Escherichia coli*: characterization of septal structure and the effects of antibiotics on cell division. *Journal of bacteriology* **119**: 303-324.

Buss, J., C. Coltharp, G. Shtengel, X. Yang, H. Hess & J. Xiao, (2015) A multi-layered protein network stabilizes the *Escherichia coli* FtsZ-ring and modulates constriction dynamics. *PLoS genetics* **11**: e1005128.

Chen, Y., K. Bjornson, S.D. Redick & H.P. Erickson, (2005) A rapid fluorescence assay for FtsZ assembly indicates cooperative assembly with a dimer nucleus. *Biophysical journal* **88**: 505-514.

Coltharp, C., J. Buss, T.M. Plumer & J. Xiao, (2016) Defining the rate-limiting processes of bacterial cytokinesis. *Proceedings of the National Academy of Sciences of the United States of America* **113**: E1044-1053.

Coltharp, C. & J. Xiao, (2017) Beyond force generation: Why is a dynamic ring of FtsZ polymers essential for bacterial cytokinesis? *BioEssays : news and reviews in molecular, cellular and developmental biology* **39**: 1-11.

Daley, D.O., U. Skoglund & B. Soderstrom, (2016) FtsZ does not initiate membrane constriction at the onset of division. *Scientific reports* **6**: 33138.

de Boer, P.A., (2010) Advances in understanding *E. coli* cell fission. *Curr Opin Microbiol* **13**: 730-737.

den Blaauwen, T., L.W. Hamoen & P.A. Levin, (2017) The divisome at 25: the road ahead. *Curr Opin Microbiol* **36**: 85-94.

Di Lallo, G., M. Fagioli, D. Barionovi, P. Ghelardini & L. Paolozzi, (2003) Use of a two-hybrid assay to study the assembly of a complex

multicomponent protein machinery: bacterial septosome differentiation. *Microbiol-Sgm* **149**: 3353-3359.

Du, S. & J. Lutkenhaus, (2017) Assembly and Activation of the *Escherichia coli* Divisome. *Molecular microbiology*.

Egan, A.J. & W. Vollmer, (2013) The physiology of bacterial cell division. *Annals of the New York Academy of Sciences* **1277**: 8-28.

Erickson, H.P., D.E. Anderson & M. Osawa, (2010) FtsZ in bacterial cytokinesis: cytoskeleton and force generator all in one. *Microbiol Mol Biol Rev* **74**: 504-528.

Fraipont, C., S. Alexeeva, B. Wolf, R. van der Ploeg, M. Schloesser, T. den Blaauwen & M. Nguyen-Disteche, (2011) The integral membrane FtsW protein and peptidoglycan synthase PBP3 form a subcomplex in *Escherichia coli*. *Microbiol-Sgm* **157**: 251-259.

Fu, G., T. Huang, J. Buss, C. Coltharp, Z. Hensel & J. Xiao, (2010) In vivo structure of the E. coli FtsZ-ring revealed by photoactivated localization microscopy (PALM). *PLoS One* **5**: e12682.

Galli, E. & K. Gerdes, (2010) Spatial resolution of two bacterial cell division proteins: ZapA recruits ZapB to the inner face of the Z-ring. *Molecular microbiology* **76**: 1514-1526.

Gerding, M.A., B. Liu, F.O. Bendezu, C.A. Hale, T.G. Bernhardt & P.A. de Boer, (2009) Self-enhanced accumulation of FtsN at Division Sites and Roles for Other Proteins with a SPOR domain (DamX, DedD, and RlpA) in *Escherichia coli* cell constriction. *Journal of bacteriology* **191**: 7383-7401.

754 Giacalone, M.J., A.M. Gentile, B.T. Lovitt, N.L. Berkley, C.W. Gunderson &
755 M.W. Surber, (2006) Toxic protein expression in *Escherichia coli* using
756 a rhamnose-based tightly regulated and tunable promoter system.
757 *Biotechniques* **40**: 355-364.
758 Gibson, D.G., L. Young, R.Y. Chuang, J.C. Venter, C.A. Hutchison & H.O.
759 Smith, (2009) Enzymatic assembly of DNA molecules up to several
760 hundred kilobases. *Nature methods* **6**: 343-U341.
761 Goehring, N.W. & J. Beckwith, (2005) Diverse paths to midcell: assembly of
762 the bacterial cell division machinery. *Curr Biol* **15**: R514-526.
763 Gustafsson, M.G.L., (2000) Surpassing the lateral resolution limit by a factor
764 of two using structured illumination microscopy. *J Microsc-Oxford* **198**:
765 82-87.
766 Haeusser, D.P. & W. Margolin, (2016) Splitsville: structural and functional
767 insights into the dynamic bacterial Z ring. *Nat Rev Microbiol* **14**: 305-
768 319.
769 Hein, B., K.I. Willig & S.W. Hell, (2008) Stimulated emission depletion (STED)
770 nanoscopy of a fluorescent protein-labeled organelle inside a living cell.
771 *Proceedings of the National Academy of Sciences of the United States*
772 *of America* **105**: 14271-14276.
773 Hjelm, A., B. Soderstrom, D. Vikstrom, W.S. Jong, J. Luirink & J.W. de Gier,
774 (2015) Autotransporter-based antigen display in bacterial ghosts.
775 *Applied and environmental microbiology* **81**: 726-735.
776 Holden, S.J., T. Pengo, K.L. Meibom, C. Fernandez Fernandez, J. Collier & S.
777 Manley, (2014) High throughput 3D super-resolution microscopy
778 reveals *Caulobacter crescentus in vivo* Z-ring organization.

Proceedings of the National Academy of Sciences of the United States of America **111**: 4566-4571.

Huecas, S., O. Llorca, J. Boskovic, J. Martin-Benito, J.M. Valpuesta & J.M. Andreu, (2008) Energetics and geometry of FtsZ polymers: nucleated self-assembly of single protofilaments. *Biophysical journal* **94**: 1796-1806.

Jacq, M., V. Adam, D. Bourgeois, C. Moriscot, A.M. Di Guilmi, T. Vernet & C. Morlot, (2015) Remodeling of the Z-Ring Nanostructure during the Streptococcus pneumoniae Cell Cycle Revealed by Photoactivated Localization Microscopy. *mBio* **6**.

Karimova, G., N. Dautin & D. Ladant, (2005) Interaction network among *Escherichia coli* membrane proteins involved in cell division as revealed by bacterial two-hybrid analysis. *Journal of bacteriology* **187**: 2233-2243.

Loose, M. & T.J. Mitchison, (2014) The bacterial cell division proteins FtsA and FtsZ self-organize into dynamic cytoskeletal patterns. *Nature cell biology* **16**: 38-46.

Meier, E.L. & E.D. Goley, (2014) Form and function of the bacterial cytokinetic ring. *Current opinion in cell biology* **26**: 19-27.

Moore, D.A., Z.N. Whatley, C.P. Joshi, M. Osawa & H.P. Erickson, (2017) Probing for Binding Regions of the FtsZ Protein Surface through Site-Directed Insertions: Discovery of Fully Functional FtsZ-Fluorescent Proteins. *Journal of bacteriology* **199**.

Muller, P., C. Ewers, U. Bertsche, M. Anstett, T. Kallis, E. Breukink, C. Fraipont, M. Terrak, M. Nguyen-Disteche & W. Vollmer, (2007) The

essential cell division protein FtsN interacts with the murein (peptidoglycan) synthase PBP1B in *Escherichia coli*. *Journal of Biological Chemistry* **282**: 36394-36402.

Ogino, H., M. Wachi, A. Ishii, N. Iwai, T. Nishida, S. Yamada, K. Nagai & M. Sugai, (2004) FtsZ-dependent localization of GroEL protein at possible division sites. *Genes to cells : devoted to molecular & cellular mechanisms* **9**: 765-771.

Ohashi, T., S.D. Galiacy, G. Briscoe & H.P. Erickson, (2007) An experimental study of GFP-based FRET, with application to intrinsically unstructured proteins. *Protein science : a publication of the Protein Society* **16**: 1429-1438.

Osawa, M., D.E. Anderson & H.P. Erickson, (2008) Reconstitution of contractile FtsZ rings in liposomes. *Science* **320**: 792-794.

Osawa, M., D.E. Anderson & H.P. Erickson, (2009) Curved FtsZ protofilaments generate bending forces on liposome membranes. *EMBO J* **28**: 3476-3484.

Osawa, M. & H.P. Erickson, (2013) Liposome division by a simple bacterial division machinery. *Proceedings of the National Academy of Sciences of the United States of America* **110**: 11000-11004.

Pazos, M., P. Natale, W. Margolin & M. Vicente, (2013) Interactions among the early *Escherichia coli* divisome proteins revealed by bimolecular fluorescence complementation. *Environmental microbiology* **15**: 3282-3291.

827 Romberg, L., M. Simon & H.P. Erickson, (2001) Polymerization of FtsZ, a
828 bacterial homolog of tubulin. is assembly cooperative? *J Biol Chem*
829 **276**: 11743-11753.
830 Rowlett, V.W. & W. Margolin, (2014) 3D-SIM super-resolution of FtsZ and its
831 membrane tethers in *Escherichia coli* cells. *Biophysical journal* **107**:
832 L17-20.
833 Rowlett, V.W. & W. Margolin, (2015) The bacterial divisome: ready for its
834 close-up. *Philosophical transactions of the Royal Society of London.*
835 *Series B, Biological sciences* **370**.
836 Schoenemann, K.M. & W. Margolin, (2017) Bacterial Division: FtsZ Treadmills
837 to Build a Beautiful Wall. *Curr Biol* **27**: R301-R303.
838 Si, F., K. Busiek, W. Margolin & S.X. Sun, (2013) Organization of FtsZ
839 filaments in the bacterial division ring measured from polarized
840 fluorescence microscopy. *Biophysical journal* **105**: 1976-1986.
841 Skoglund, U., L.G. Ofverstedt, R.M. Burnett & G. Bricogne, (1996) Maximum-
842 entropy three-dimensional reconstruction with deconvolution of the
843 contrast transfer function: a test application with adenovirus. *J Struct*
844 *Biol* **117**: 173-188.
845 Söderström, B. & D.O. Daley, (2017) The bacterial divisome: more than a
846 ring? *Current genetics* **63**: 161-164.
847 Söderström, B., K. Mirzadeh, S. Toddo, G. von Heijne, U. Skoglund & D.O.
848 Daley, (2016) Coordinated disassembly of the divisome complex in
849 *Escherichia coli*. *Molecular microbiology* **101**: 425-438.
850 Söderström, B., K. Skoog, H. Blom, D.S. Weiss, G. von Heijne & D.O. Daley,
851 (2014) Disassembly of the divisome in *Escherichia coli*: evidence that

FtsZ dissociates before compartmentalization. *Molecular microbiology* **92**: 1-9.

Strauss, M.P., A.T.F. Liew, L. Turnbull, C.B. Whitchurch, L.G. Monahan & E.J. Harry, (2012) 3D-SIM Super Resolution Microscopy Reveals a Bead-Like Arrangement for FtsZ and the Division Machinery: Implications for Triggering Cytokinesis. *PLoS biology* **10**.

Szwedziak, P., Q. Wang, T.A. Bharat, M. Tsim & J. Lowe, (2014) Architecture of the ring formed by the tubulin homologue FtsZ in bacterial cell division. *Elife* **3**: e04601.

Trip, E.N. & D.J. Scheffers, (2015) A 1 MDa protein complex containing critical components of the *Escherichia coli* divisome. *Scientific reports* **5**: 18190.

Vicidomini, G., G. Moneron, K.Y. Han, V. Westphal, H. Ta, M. Reuss, J. Engelhardt, C. Eggeling & S.W. Hell, (2011) Sharper low-power STED nanoscopy by time gating. *Nature methods* **8**: 571-573.

Vicidomini, G., A. Schonle, H. Ta, K.Y. Han, G. Moneron, C. Eggeling & S.W. Hell, (2013) STED nanoscopy with time-gated detection: theoretical and experimental aspects. *PLoS One* **8**: e54421.

Weiss, D.S., (2015) Last but not least: new insights into how FtsN triggers constriction during *Escherichia coli* cell division. *Molecular microbiology* **95**: 903-909.

Wissel, M.C. & D.S. Weiss, (2004) Genetic analysis of the cell division protein FtsI (PBP3): amino acid substitutions that impair septal localization of FtsI and recruitment of FtsN. *Journal of bacteriology* **186**: 490-502.

Xiao, J. & E.D. Goley, (2016) Redefining the roles of the FtsZ-ring in bacterial cytokinesis. *Current Opinion in Microbiology* **34**: 90-96.

Yang, X., Z. Lyu, A. Miguel, R. McQuillen, K.C. Huang & J. Xiao, (2017) GTPase activity-coupled treadmilling of the bacterial tubulin FtsZ organizes septal cell wall synthesis. *Science* **355**: 744-747.

Yao, Q., A.I. Jewett, Y.W. Chang, C.M. Oikonomou, M. Beeby, C.V. Iancu, A. Briegel, D. Ghosal & G.J. Jensen, (2017) Short FtsZ filaments can drive asymmetric cell envelope constriction at the onset of bacterial cytokinesis. *EMBO J*.

Figures legends

Figure 1. Radial separation of FtsZ and FtsN during constriction of the cell envelope in *E. coli*. (**A**) Cells engineered to express fluorescently labeled division proteins were trapped in micron-sized holes in agarose beds so that divisome proteins could be imaged through the longitudinal axis of the cell. For more information see Supporting Information Fig. S1. Cells co-expressing (**B**) FtsZ-GFP/mCherry-FtsN (n = 51), (**C**) FtsZ-mNG/mCherry-FtsN (n = 72), (**D**) ZipA-GFP/mCherry-FtsN (n = 54) and (**E**) GFP-FtsI/mCherry-FtsN (n = 30) were trapped in microholes and imaged by SIM. Left column shows cells where the radius of the division ring was > 450 nm. Right column, cells where the radius of the division ring was < 450 nm. Next to each image are the corresponding fluorescence intensity line scans. These scans start at 9 o'clock in each image (see red triangle in (**B**)) Scale bars = 0.5 µm. (**F**) Comparison between the radius of mCherry-FtsN and either FtsZ-GFP or ZipA-GFP (n > 45). Trend line for FtsZ-GFP /mCherry-FtsN; y = 0.89x + 72.2 ($r_{Pearson}$ = 0.973, p < 0.05). Trend line for ZipA-GFP /mCherry-FtsN; y = 0.86x + 91.7 ($r_{Pearson}$ = 0.982, p < 0.05). n > 50 for both pairs. (**G**) Comparison between GFP-FtsI and mCherry-FtsN radii throughout constriction. Trend line mCherry-FtsN/GFP-FtsI; y = 1.01x+0.42 ($r_{Pearson}$ = 0.999, p < 0.05). n = 30. (**H**) Summary of the separation between various divisome proteins during different stages of constriction. y-axis shows average difference in radius between mCherry-FtsN and respective protein (in nm). Bar graphs show averaged data; At least 50 cells from FtsZ-GFP /mCherry-FtsN and 30 cells from ZipA-GFP /mCherry-FtsN. Error bars indicate SEM. All strains had

comparable lengths and widths to a wild type strain and their generation times appeared unaffected. Controls for cell length, width and growth can be found in Supporting Information Fig. S2.

Figure 2. Separation between FtsZ and FtsN resolved at nanometer scale by dual-color gSTED. (**A**) Cells co-expressing FtsZ-mNG and mStrawberry-FtsN were trapped in microholes, fixed and imaged by dual-color gSTED. Red arrow indicates the start of the fluorescence line trace. The graph on the right-hand panel shows the intensity of each fluorescent protein around the circumference of the division site. For comparison, a representative line in a live/unfixed cell is shown in Supporting Information Fig. S8. (**B**) Close up images of a ring section highlighting areas where the fluorescence signals from FtsZ-mNG and mStrawberry-FtsN were the same radii but not overlapping. Dotted white line indicates fluorescence line trace, starting at the red arrow. (**C**) Close up images of a ring section where FtsZ-mNG and mStrawberry-FtsN have constricted to different radii. Differences are highlighted through fluorescence line traces in the graphs. Line (1) shows FtsZ densities aligned along the circumference of the membrane. Line (2) shows a density that is perpendicular to the membrane. Positive x direction indicates increasing radii. (**D - G**) Pseudo time-lapse images of cells co-expressing FtsZ-mNG and mStrawberry-FtsN. The cells were trapped in microholes and imaged by dual-color gSTED. Radii denoted are those measured for FtsZ-mNG. Scale bars (**A**) and (**D - G**) = 0.5 μm, (**B**) and (**C**) = 0.1 μm

Figure 3. Septal organization of divisome proteins revealed by gSTED. (**A**) Cells expressing FtsZ-mNG were trapped in microholes, fixed and imaged at different stages of constriction by gSTED. For comparison, live/unfixed cells are shown in Supporting Information Fig. S10. (**B**) Distribution of fluorescent density lengths obtained from gSTED images of FtsZ-mNG (n = 55). (**C**) An example of an FtsZ-mNG density that was not positioned along the circumference of the cell. (**D**) Wild type cells were fixed and then trapped in microholes. FtsZ was subsequently labelled using anti-sera and imaged at different stages of constriction by gSTED. (**E**) Distribution of fluorescent density lengths obtained from gSTED images of antibody labeled FtsZ (n = 51). (**F**) An example of a density that was not positioned along the circumference of the cell. (**G**) Cells expressing mCitrine-FtsN were trapped in microholes, fixed and imaged at different stages of constriction by gSTED. (**H**) Distribution of fluorescent density lengths obtained from gSTED images of mCitrine-FtsN (n = 59). (**J**) An example of mCitrine-FtsN density that was not positioned along the circumference of the cell. (**K**) Wild type cells were fixed and then trapped in microholes. FtsN was labelled using anti-sera and imaged at different stages of constriction by gSTED. (**L**) Distribution of fluorescent density lengths obtained from gSTED images of antibody labeled FtsN (n = 53). (**M**) Close up of typical arrangement of native FtsN densities along the circumference of the ring. (**N**) Summary of measured density lengths. (**O**) Average ring coverage in % of FtsZ and FtsN at septum in unconstricted cells (100 % would indicate full ring coverage). FP = Fluorescent Protein. IFM = Immunofluorescence. For consistency all images were pseudo-colored green irrespectively of their emission wavelength. Bin width for the histograms in

(**B**), (**E**), (**H**) and (**L**) is 25 nm. Full Width at Half Maximum (FWHM) in the graphs indicates the thickness of the filament. Scale bars = 0.5 μm.

Figure 4. FtsN moves around the division septum even after it has separated from FtsZ. Cells simultaneously expressing FtsZ-GFP and mCherry-FtsN were analyzed using time-lapse SIM. (**A**) Representative images of a cell with overlapping fluorescence signals. (**B**) Representative images a cell where signals did not overlap. Numbers in top right corners indicate the time after the first shown image. Next to each image are 3D surface plots that highlight the variation in fluorescence intensity along the circumference of the rings between each time point. See also Supporting Movies S1 and S2.

Figure 5. Different modes of subunit exchange between FtsZ and FtsN at septum. (**A**) Confocal FRAP measurements of cells simultaneously expressing FtsZ-mNG and mCherry-FtsN. The boxed region was photo-bleached and the recovery of fluorescence monitored at times indicated. Recovery curves for FtsZ-mNG (green) and mCherry-FtsN (red) are shown in (**B**). (**C**) Quantification of recovery times for bleached half-rings of various divisome proteins. Examples of raw data are shown in Supporting Information Fig. S15. (**D**) Following bleaching the reappearance of FtsZ-GFP in filaments was tracked over time. These filaments reappeared throughout the bleached areas (see also Supporting Movie S5). (**E**) As for panel D except that FtsZ-mNG was used. (**F**) After bleaching the reappearance of mCitrine-FtsN was monitored over time. The fluorescence reappeared throughout the bleached

areas (i.e. no transient filament like structures were observed). Scale bars = 0.5 μm.

Figure 6. Increasing radial distance between FtsZ and FtsN during constriction. Model depicting how the spatial difference between FtsZ and FtsN changes with constriction of the septum. (**A**) Prior to the initiation of constriction the radii of the two 'rings' essentially overlap. However, the FtsZ filaments and FtsN assemblies do not always co-localize circumferentially. (**B**) As constriction of the cell envelope advances, the radial difference between FtsZ and FtsN increases to, on average, 50 nm. OM, outer membrane; IM, inner membrane; PG, peptidoglycan.

Figure 1

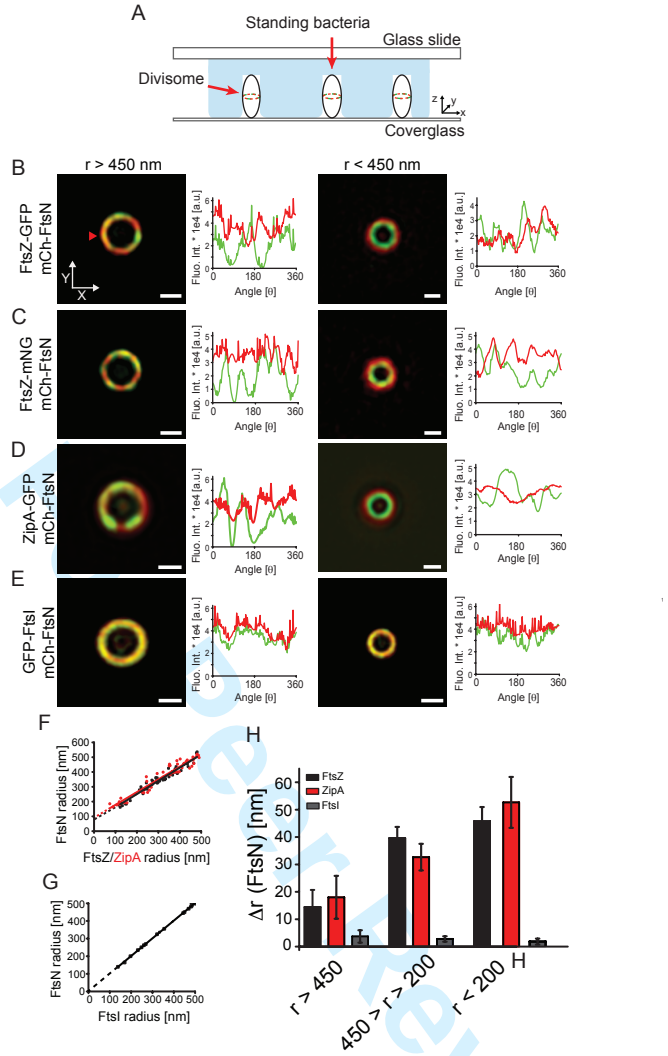

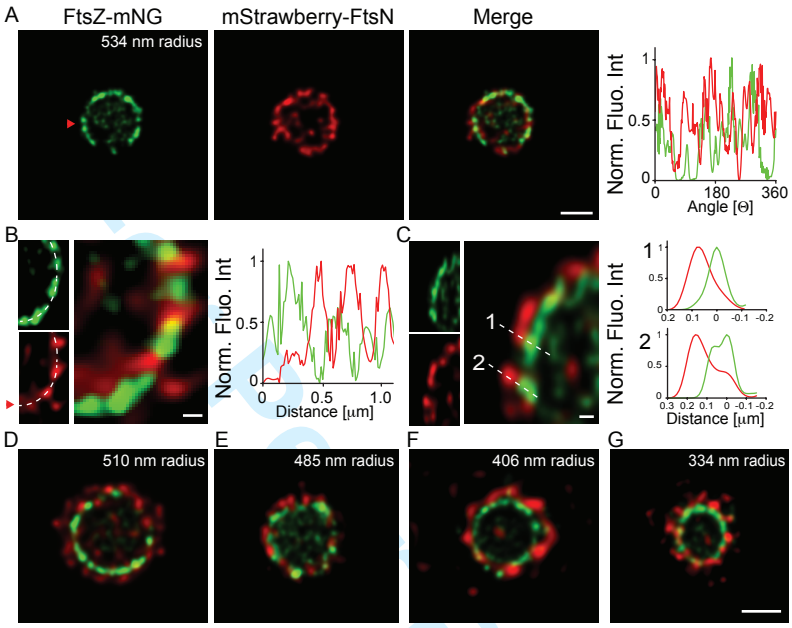

Figure 3

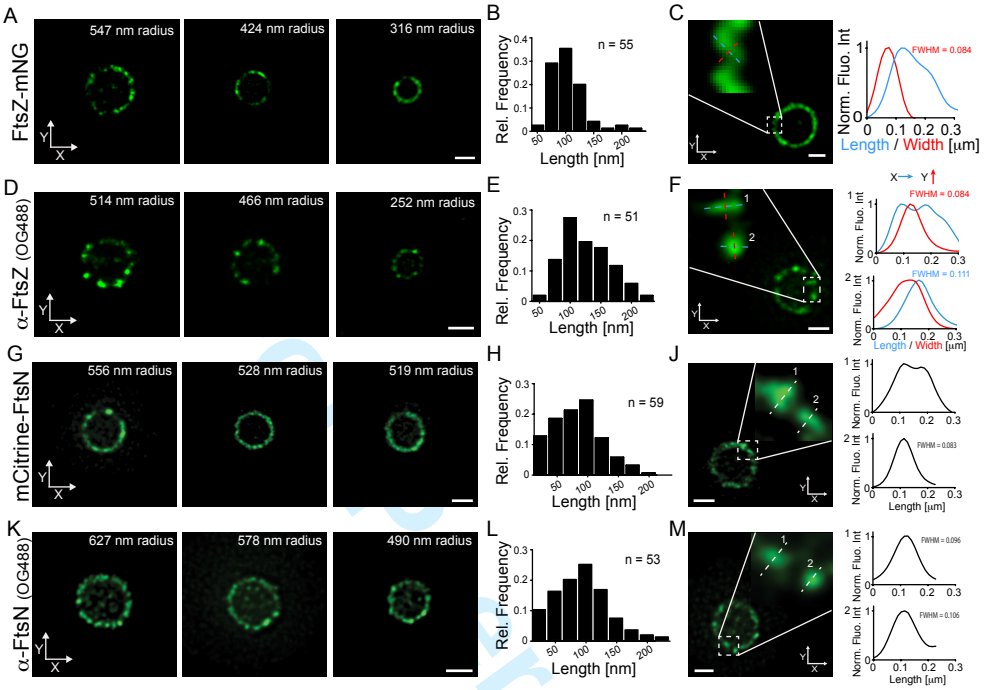

% full ring	FtsZ	FtsN
FP	65 ± 12	79 ± 7
IFM	53 ± 8	81 ± 4

Mean ± S.D.

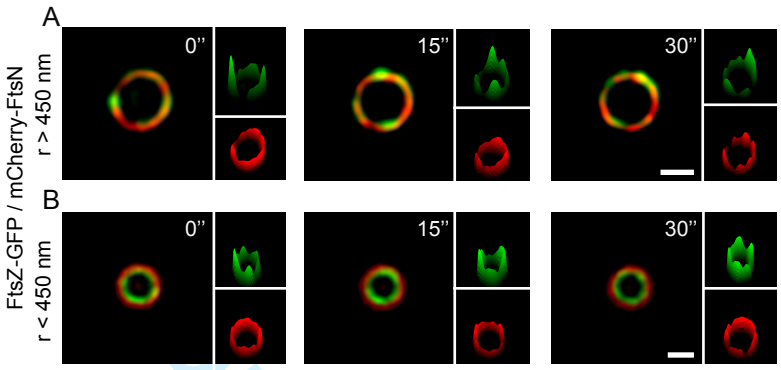

Figure 5

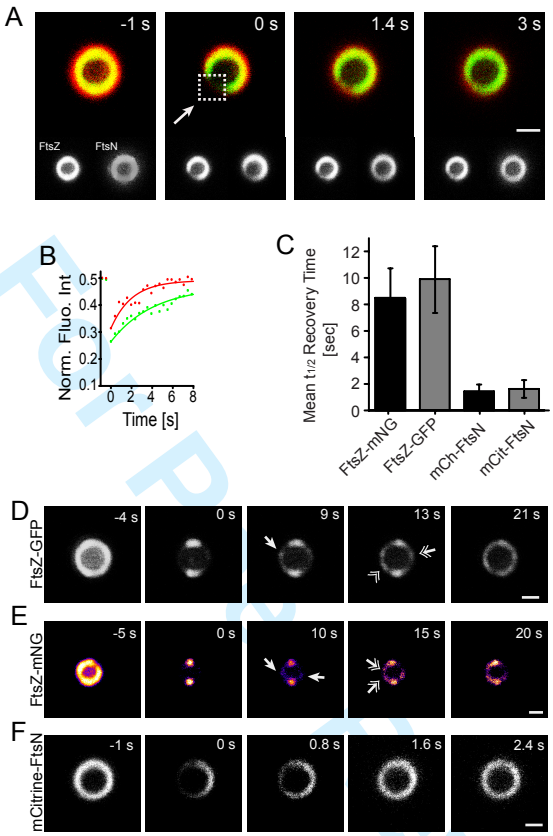

Figure 6

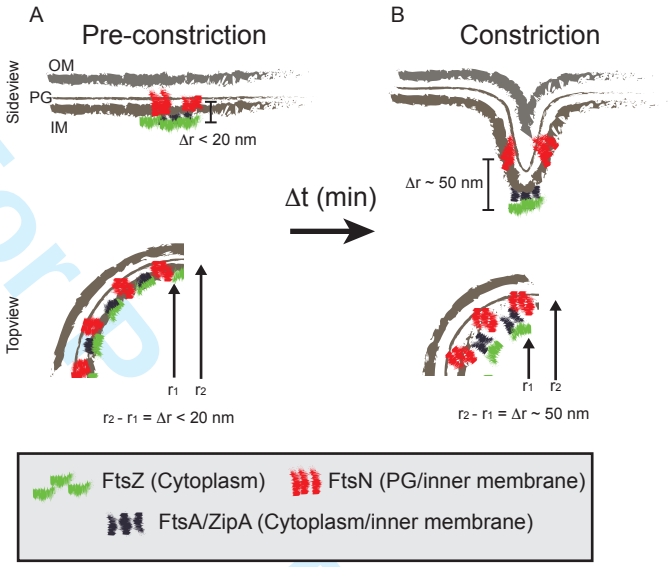

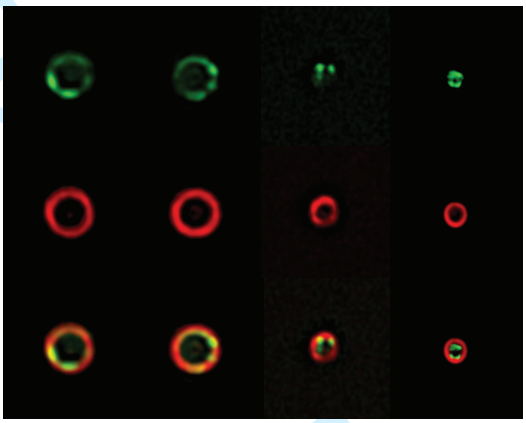

Abbreviated summary

In order to divide, bacterial cells assemble a macromolecular machine, termed ‘the divisome’. Herein we used super-resolution microscopy investigate the organization of two key divisome proteins; FtsZ and FtsN. We found that these proteins were both circumferentially and radially separated into individual protein assemblies. Thus, our data indicates that division is brought about by a collection of independently operating protein assemblies, rather than a single macromolecular machine.

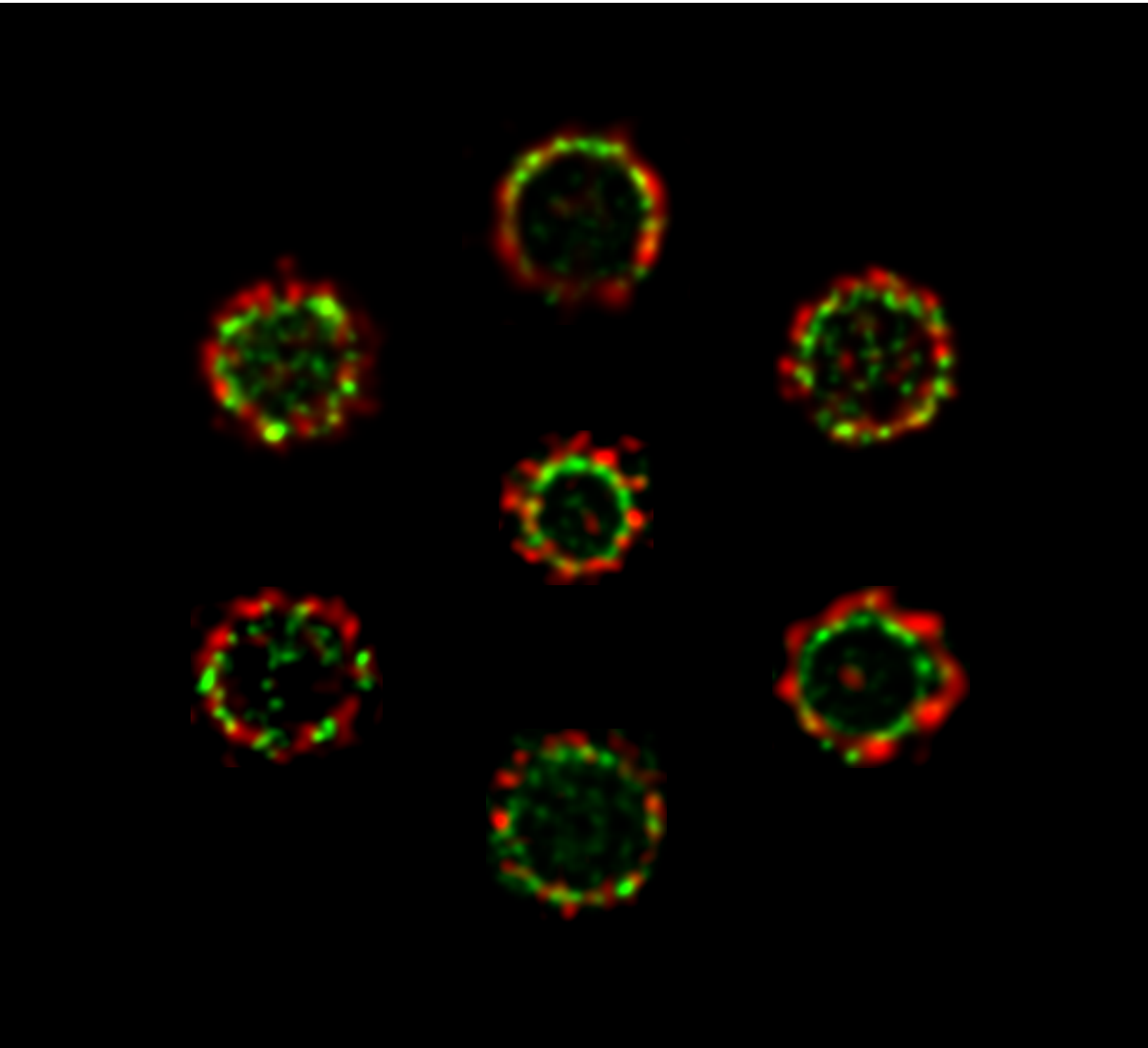

A montage of images through the division septum of *E. coli* cells. The images were captured by dual-color time-gated Stimulated Emission Depletion (STED) nanoscopy, on cells simultaneously expressing FtsZ-mNeonGreen (green) and mStrawberry-FtsN (red). The images show that FtsZ and FtsN are spatially separated.